



The synthesis and properties of ZnO–graphene nano hybrid for photodegradation of organic pollutant in water

Dongying Fu, Gaoyi Han*, Yunzhen Chang, Jianhua Dong

Institute of Molecular Science, Key Laboratory of Chemical Biology and Molecular Engineering of Education Ministry, Shanxi University, Taiyuan 030006, PR China

ARTICLE INFO

Article history:

Received 4 July 2011

Received in revised form 5 November 2011

Accepted 30 November 2011

Keywords:

Graphene

ZnO

Photodegradation

Methylene blue

Photocatalysis

ABSTRACT

The nano-sized zinc oxide–graphene oxide (ZnO–GO) hybrid has been prepared by using GO dispersed in the ethanol as carrier, zinc acetate dihydrate and lithium hydroxide monohydrate as reactant. Then the nano-sized hybrid material of ZnO–graphene (ZnO–G) is obtained by thermally treating ZnO–GO at different temperatures. The samples are characterized by using scanning and transmission electron microscopy, X-ray diffraction, X-ray photoelectron spectroscopy, Raman, electron absorption and photoluminescence emission spectroscopy. The results reveal that both sides of the graphene sheets are coated with ZnO particles, and that the lattice constants and the band gap energy of ZnO have been changed compared with the pure nano-sized ZnO particles. The photodegradation of methylene blue (MB) has been investigated in the presence of hybrid materials. It is found that ZnO–G prepared at 200 °C containing 2.5% graphene exhibits the highest activity which is three times as large as that of pure ZnO. The optimum ZnO–G catalyst still retains the 80% of the initial activity still after it has been used 5 times repeatedly, and exhibits larger rate for MB degradation than pure ZnO in each recycled time.

© 2011 Elsevier B.V. All rights reserved.

1. Introduction

Recently, great interest has been stimulated in the treatment of organic contamination in water through photocatalytic method because it can destruct the pollutants completely and has a broad optional compound [1–3]. Among the semiconductors used as photocatalyst, TiO₂ has been widely used for complete degradation of the recalcitrant organic pollutants because of its high efficiency, nontoxicity and photochemical stability [2,3].

ZnO, as a semiconductor, is also usually used as photocatalyst to destroy the organic pollutants in water or air because its high photo-sensitivity and large band gap can offer the high driving force for reduction and oxidation processes [4]. It is proved that ZnO may exhibit a better efficiency than TiO₂ in photocatalytic degradation for some dyes [5]. Usually, the photocatalytic activity of the catalyst can be influenced strongly by the crystal structure, particle size, dispersibility, band gap and the hydroxyl density on the surface [6–9]. Furthermore, the catalytic efficiency and the applied scope of the photo-catalyst may be limited by two facts: (1) charge carrier recombination occurs within a short time as nanoseconds, and (2) the band edge absorption threshold does not allow the utilization of visible light [6]. The attempt has been made to improve dispersibility of ZnO by loading the particles on the sepiolite [10] which prevents the particles from aggregation, but the recombination of

the photo-generated electrons and holes cannot be reduced by dispersing on it. Therefore, several methods have been employed to reduce the recombination of charge carriers by coupling the photocatalysts with noble metals [11], semiconductors [12], polyaniline [13] and carbonaceous materials such as carbon nanotubes and C₆₀ [13–16], which can take the role of electron scavenging agents. However, neither the CNT nor C₆₀ is suitable to be extensively used now for their high price [17].

As a new kind of two-dimensional carbon material constructed by single layer of carbon atoms, graphene is an excellent supporting and electron-transport material compared with other carbon materials in the process of photocatalysis for its large surface area, superior electrical conductivity and mechanical properties [18,19]. Furthermore, graphene can be easily produced from inexpensive natural graphite through intermediates product graphite oxide (GO). Besides, the presence of oxygen-containing functional groups in GO and reduced GO will make them excellent supporting material to anchor nanocrystals during the process of synthesis [20]. Up to the date, efforts have been made to utilize graphene to improve the efficiency of photocatalysts [21–26] and solar cells [27–29]. Furthermore, the composite of ZnO and graphene has been synthesized by treating the mixture of ZnO particles and GO through hydrothermal process or co-precipitation; however, the structural changes such as lattice constants and band gap energy of ZnO have not been observed in the composite [17,30].

It has been proved that ZnO nanoparticles can be conveniently prepared by using the zinc acetate dihydrate and lithium hydroxide monohydrate as reactants in ethanol medium. It is expected that

* Corresponding author. Tel.: +86 351 7010699; fax: +86 351 7016358.
E-mail address: han_gaoyis@sxu.edu.cn (G. Han).

the GO can contact with ZnO more intimately when the ethanol dispersion of GO exists synchronously. The hybridization of ZnO with graphene will increase the dispersibility of the catalyst and reduce the recombination of charge carriers, which is favorable to increase the photocatalytic efficiency. In present work, the hybrid of ZnO–G will be prepared by thermal treatment of the ZnO–GO prepared in ethanol system containing different amount of GO sheets, and the photocatalytic property of the hybrid will also be investigated in detail.

2. Experimental

2.1. Materials

Natural mineral graphite powder (NGP, 99.9%, 325 mesh) was obtained from the Tianjin Guangfu Research Institute. GO was prepared from NGP according to the previous method [31,32]. P25 (TiO₂) was obtained from Evonik Degussa (Hualisen Guangzhou). LiOH·H₂O (95%), Zn(CH₃COO)₂·2H₂O (99%), n-hexane (98%), H₂O₂ (30%), sulfuric acid (H₂SO₄, 98%), chlorohydric acid (HCl, 36%) and other chemicals were of AR grade. Unless otherwise specified, all reagents and materials involved were used as received without further purification. Anhydrous ethanol was refluxed over CaO for 2 h and distilled before use. Methylene Blue (MB) was obtained from Zhangjiagang Chemical Plant. The GO stock dispersion was prepared by dispersing 20.0 mg GO in 10.0 mL ethanol to form 2.0 mg mL⁻¹ dispersion.

2.2. Preparation of ZnO–graphene hybrid

ZnO nanoparticles were synthesized according to the method reported previously [10,33]: 1.10 g (5.0 mmol) sample of Zn(CH₃COO)₂·2H₂O was dissolved into 50.0 mL anhydrous ethanol at 80 °C under vigorous stirring for about 20 min; after the mixture was cooled to 50 °C, LiOH·H₂O (0.30 g) dissolved in other 50.0 mL anhydrous ethanol containing a certain amount of GO dispersion was added into the solution of Zn(CH₃COO)₂·2H₂O; the mixture was then kept under vigorous stirring for 40 min, in which the resulted ZnO particles were supported on the surface of the GO sheets. After cooling, more than twice as much hexane in volume was added to the mixture and stored at temperature under 4 °C overnight. The precipitate was collected by filtering the mixture through the micro-porous filter membrane and washed by deionized water and ethanol thoroughly to remove the impurity after being dried under vacuum at 50 °C and designated as ZnO–GO. The samples were designated as ZnO–G after they were thermally treated for 2.0 h in a tube furnace at different temperatures under high-purity Argon atmosphere. By comparison, the composite ZnO-multiwalled carbon nanotube (ZnO–MWCNT) and pure ZnO nanoparticles were also synthesized according to the similar procedure.

2.3. Characterization of the composites

The XRD patterns of the samples were recorded on a Bruker D8 Advance X-ray diffraction meter with Cu K α radiation and graphite monochromator, at the scan speed of 5°/min with a step size of 0.02°. The morphologies of the samples were observed by using a JEOL-JSM-6701 field-emission scanning microscope (SEM) operating at an accelerating voltage of 10 kV and a JEOL 2010 transmission electron microscopy (TEM) operating at 200 kV. X-ray photoelectron spectroscopy (XPS) measurements were performed with an ESCALAB 220i-XL spectrometer (VG Scientific, England) employing a monochromic Al K α source at 1486.6 eV. Raman spectra were recorded on a JobinYvon Lab RAMHR800 microscopic confocal Raman spectrometer by employing laser of 514 nm as incident

light. The thermogravimetric analysis (TGA) was performed on a STA449C thermo gravimetric analyzer from room temperature to 800 °C with a heating rate of 10 °C min⁻¹. The photo-activity of the samples and the UV–visible spectra were measured on a Varian 50 Bio UV–visible spectrophotometer and the fluorescence properties of the samples were investigated on a Hitachi F-2500 spectrofluorometer at room temperature. The electrochemical impedance spectra (EIS) measurements were carried out on a CHI 660C electrochemical workstation (Chenhua, Shanghai) by using three-electrode system.

2.4. Photocatalytic activity of the composites

The photodegradation process of MB was tracked based on the absorption spectroscopic technique. In a typical process, the solution of the MB (20.0 mg L⁻¹, 50.0 mL) containing a certain amount of the photo-catalyst in a 100 mL beaker was stirring for 30 min under dark at ambient conditions to get the absorption–desorption equilibrium before irradiation. Then the beak was exposed to the light irradiation produced by a 200 W Xe lamp positioned 36 cm away from the vessel. The photo-catalytic reaction started from turning on the Xe lamp, and during the photocatalysis, the degradation solution was analyzed by recording variations of the absorption located at maximum band at given time intervals. During the photodegradation, the temperature was kept at about 25 °C and the pH value of the dispersion was kept at about 6.5. After given time intervals, 1.0 mL of the mixture under radiation was transferred from the vessel and was centrifuged at 12,000 rpm for 3 min to remove the catalyst particles completely. The absorbency of the MB solution was measured in the mixture of ethanol and water with a volume ration of 3:1. The control experiments such as irradiating without photo-catalyst or non-irradiating in the presence of photo-catalyst were also carried out at the similar procedure. The durability test of the catalyst in the photo-degradation of MB under light radiation was performed following the same procedure, at the beginning, 30.0 mg of ZnO–G or ZnO was dispersed in 50.0 mL MB solution with the concentration of 20.0 mg L⁻¹, and then the mixture underwent five consecutive cycles, each lasting for 70 min. After each cycle, the catalyst was centrifuged and washed thoroughly with water, and then fresh MB solution was added to the catalyst.

2.5. Fabrication of the electrodes for EIS measurements

For the EIS measurement, the photo-catalyst (5.0 mg) was dispersed in 1.0 mL ethanol, then 50 μ L dispersion was dropped on a carbon electrodes for five times. The EIS measurements were carried out on a CHI 660C electrochemical workstation by using three-electrode cells after drying in air at 100 °C. The resultant electrode served as the working electrode, with a platinum plate and a saturated calomel electrodes (SCEs) as the counter and reference electrodes, which was performed in the presence of a 2.5 mM K₃[Fe(CN)₆]/K₄[Fe(CN)₆] (1:1) mixture as redox probe in 0.1 M KCl solution. The impedance spectra were recorded under an ac perturbation signal of 10 mV over the frequency range of 10⁵–0.1 Hz.

3. Results and discussion

3.1. Characterization of the hybrids

The XRD patterns of the samples are shown in Fig. 1, it is found that all the samples present the typical XRD diffraction character of wurtzite structure according to the standardized JCPDS (36-1451) card. However, no characteristic peaks are observed for either GO or graphite in the corresponding region, which may arise from the factors that the content of the graphene is low and that the

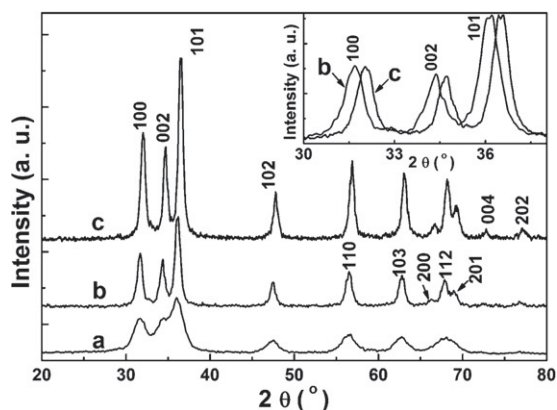


Fig. 1. The XRD patterns of pure ZnO and ZnO-G containing 2.5% graphene. (a) ZnO-GO as prepared; (b) ZnO-G calcined at 200 °C and (c) pure ZnO calcined at 200 °C.

deposited ZnO particles prevent the graphene sheets from forming the inert stacks [32]. The sample of ZnO-GO (Fig. 1a) shows the similar broader diffraction peaks to the pure ZnO as prepared, which indicates that the size of ZnO particles is smaller. Furthermore, the diffraction peaks of the ZnO-G (Fig. 1b) are shifted to small degree (Fig. S1) compared with that of pure ZnO (Fig. 1c), which indicates that the lattice constants of ZnO have changed because of the presence of the carbonaceous material. It is different from the results reported previously where the presence of graphene has no influence on lattice constants of the ZnO [17,30]. Therefore it can be concluded that the interaction between the GO or graphene and ZnO particles is stronger in present work. The particles' sizes are estimated by employing Debye–Scherrer's formula based on the diffraction peak corresponding to the (101) plane, and the lattice constants (a , b and c) can be calculated according to Bragg's law $2d\sin\theta = n\lambda$. The lattice constants are given by [34]

$$a = b = \frac{\lambda}{\sqrt{3}\sin\theta} \text{ and } c = \frac{\lambda}{\sin\theta} \quad (2)$$

according to the (100) and (002) plane orientation, respectively. From the data listed in Table 1, it is found that the average crystal size of ZnO-GO and ZnO-G is smaller than that of ZnO as prepared and calcined at 200 °C, respectively. The lattice constants in ZnO-GO and ZnO-G are larger than that in pure ZnO, indicating that the presence of GO or graphene can make the lattice constants of ZnO larger and stabilize the particles.

Table 1

The physical properties of the ZnO crystallite prepared in this work.

Samples	d (nm)	a (Å)	c (Å)	V (Å ³)	E_g (eV)
ZnO	5.8	3.231	5.170	46.741	3.29
ZnO-GO	5.6	3.261	5.227	48.138	3.31
ZnO ^a	16.4	3.225	5.172	46.585	3.29
ZnO-G ^a	12.9	3.263	5.224	48.169	3.26

d is the crystal size calculated by plane (101), a and c are calculated based on the plane (100) and (002), E_g is obtained based on the absorption spectroscopy.

^a The sample is prepared by being thermally treated at 200 °C.

In order to clarify the evolution of the GO in the hybrids, the XPS spectra of GO and the composites prepared at different temperature are shown in Fig. 2. Curve fitting of the XPS peaks can be performed using Gauss–Lorentzian peak shape after performing a Shirley background correction. The C1s peak with a binding energy of 284.5 eV can be attributed to the C–C and C=C bonds, and the fitted peaks with binding energy of 286.5, 287.2 and 288.7 eV are typically assigned to C–OH, C=O and O=C–OH functional groups (Fig. 2A-a), respectively [35–38]. Most structural models of GO also include an epoxide group (C–O–C), which should have a C1s binding energy similar to C–OH [38]. The peak with the binding energy of 283.6 eV can be assigned to the C–M bond (Fig. 2A-d), which indicates that the bond between C and Zn has formed at higher temperature (500 °C). It can be calculated that the relative ratio of the areas of C1s peaks related to the C–C and C–O ($R_{cc/co}$) is about 0.75 in the GO spectrum, and that the values of $R_{cc/co}$ increase to about 4.17, 4.35 and 6.25 after the prepared ZnO-GO hybrids are thermally treated at 100, 200 and 500 °C. It is surprising to find that the value of $R_{cc/co}$ reaches to 4.17 when the sample of ZnO-GO is treated at 100 °C. The O1s XPS peak located at 532.4 eV (Fig. 2B-a) is wide and almost symmetric (Fig. 2B), which can be attributed to the oxygen of hydroxyl and epoxide, carbonyl and carboxyl group in GO [35,38]. However, the O1s XPS peaks of the samples of ZnO-G are asymmetrical and present a visible shoulder, the peak centered at 529.8 eV is attributed to the O ion in ZnO lattice, the peak at 531.3 eV is associated with O ions in oxygen-deficient lattice in ZnO, and the peaks located at about 532.2 eV may be attributed to the chemisorbed oxygen species [39].

The Raman spectra of pristine GO and ZnO-G are shown in Fig. 3, from which it can be found that the GO (Fig. 3a) shows the D and G bands at 1348 and 1586 cm⁻¹. The G band is attributed to all sp² carbon forms and provides information on the in-plane vibration of sp² bonded carbon atoms while the D band suggests the presence of sp³ defects [35]. The peak at 2685 cm⁻¹ is corresponding to the overtone of the D band, and the peak at 2927 cm⁻¹ is associated

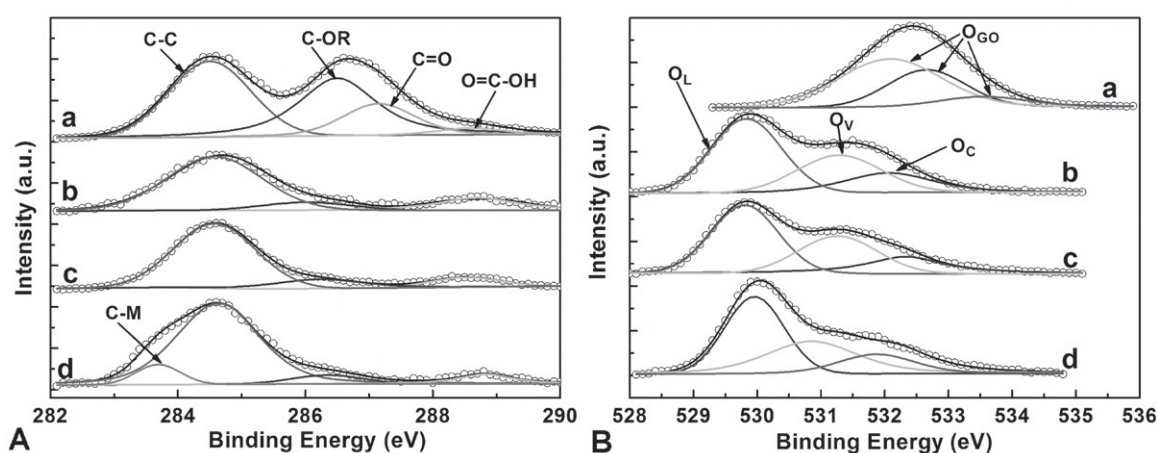


Fig. 2. The C1s (A) and O1s (B) XPS spectra of the GO and ZnO-GO treated at various temperatures. (a) GO, (b) ZnO-GO (c) and (d) the ZnO-G prepared at 200 and 500 °C.

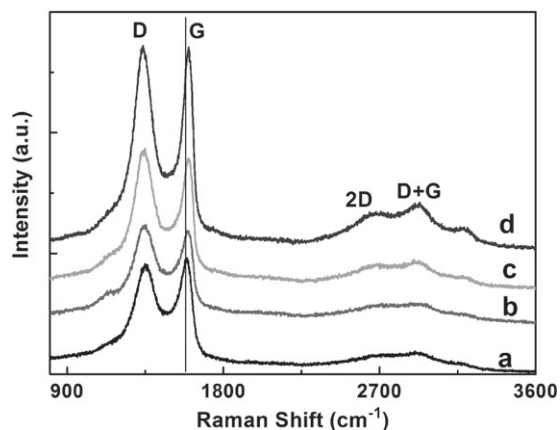


Fig. 3. The Raman spectra of the GO (a), ZnO-GO (b), ZnO-G prepared at 200 °C (c) and 500 °C (d).

with the *D* + *G* band [36]. The samples of ZnO-G (Fig. 3b–d) present the similar spectra to GO. The ratios of the area of *D* band and *G* band ($R_{AD/AG}$) are calculated to be about 2.35, 2.80, 2.68 and 2.68 for GO and ZnO-GO thermally treated at 100, 200 and 500 °C, respectively. The accompanying increase of the $R_{AD/AG}$ values for ZnO-G can be explained by the presence of smaller but more numerous sp^2 domains during the heating process of the GO [40]. It is worth noting that a *G* band up-shift from 1586 to 1599 cm^{-1} is observed for ZnO-G compared with GO. This *G* band shift is generally given as evidence for chemical doping of the carbon materials [41]. The above mentioned XPS and Raman spectra also provide reliable evidence for the stronger interaction between the ZnO and graphene sheets.

TGA is an effective analytical technique to evaluate the content of the graphene in the hybrid of ZnO-G. From Fig. 4, it can be found that the mass loss of GO is about 13% from 25 to 125 °C because of the adsorbed water loss. The dramatic mass loss initiated at about 198 °C can be contributed to the decomposition of the oxygen group

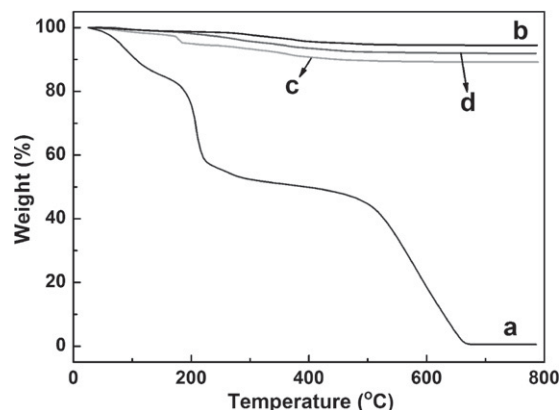


Fig. 4. TGA curves of GO (a), pure ZnO calcined at 200 °C (b), ZnO-GO thermally treated at 100 °C (c) and ZnO-G prepared at 200 °C (d).

in GO, and the mass loss from 125 to 300 °C is about 35%. The mass loss at above 300 °C can be attributed to the carbon oxidation, and the complete decomposed temperature of the residue carbon is about 702 °C (Fig. 4a). However, the TGA curve of ZnO-GO shows a dramatic mass loss at 174 °C, which is a lower decomposition temperature for oxygen group compared with GO, indicating that the thermal stability of GO is decreased after composited with ZnO (Fig. 4c). The curve of pure ZnO calcined at 200 °C shows a total mass loss of about 5.5% at 800 °C because of the adsorbed water and acetate group (Fig. 4b). However, the ZnO-G prepared at 200 °C with certain GO content shows a total mass loss of about 8.0% at the same temperature (Fig. 4d). Therefore, the content of graphene in ZnO-G can be deduced according to the curves b and d and found to be about 2.5%.

From the typical SEM images of ZnO-GO as prepared shown in Fig. 5A, it can be seen that both sides of the GO sheets are closely coated with the particles of ZnO (the average size is roughly 5 nm) in relatively high density to form a sandwich-structure stacks layer upon layer. The ZnO-G prepared at 200 °C containing 2.5% graphene

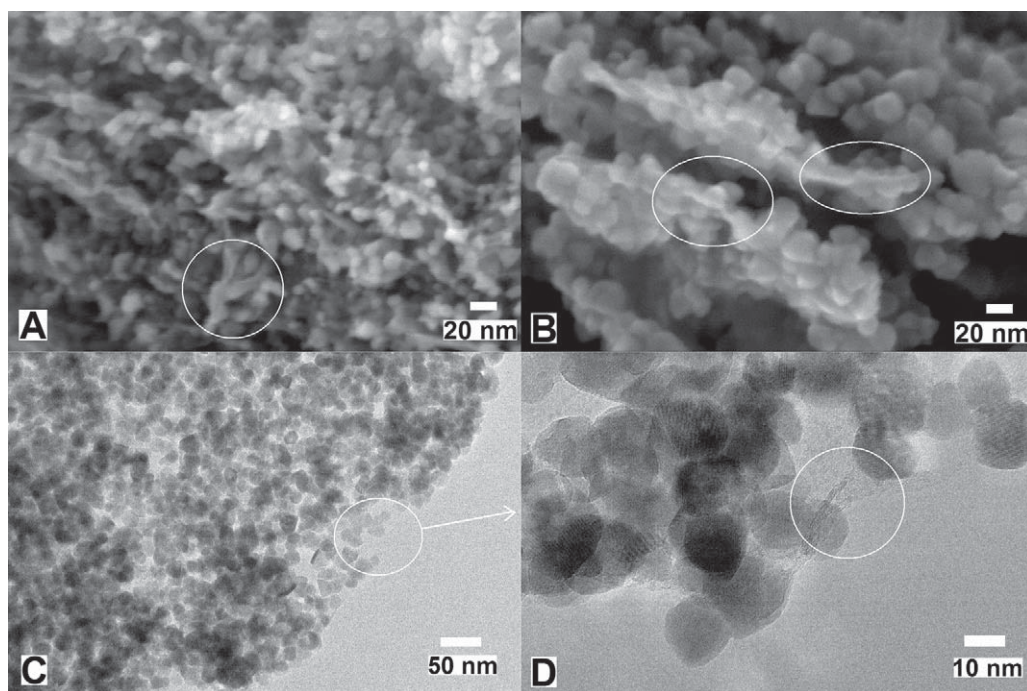


Fig. 5. The SEM images of ZnO-GO as prepared (A) and ZnO-G prepared by thermally treated ZnO-GO at 200 °C, (C) the TEM image of ZnO-G as shown in (B) and (D) the magnified TEM image shown in (C).

still retains the sandwich-structure except that the size of the ZnO particles increases to roughly 14 nm (Fig. 5B). From the TEM images of ZnO–G shown in Fig. 5C, it is found that ZnO particles assemble on the graphene sheets in a relatively high density. From the magnified TEM image shown in Fig. 5D, it can be seen that the graphene sheets are not perfectly flat but intrinsically microscopic rough and out of plane deformations (wrinkles), and that some very small particles are also observed on the surface of graphene, which is similar to the results reported previously where subnanosized Pt particles are observed on the graphene surface besides the nano-sized Pt particles [42]. The intimate contact between ZnO and graphene will make the strong electronic interaction between ZnO and graphene possible, and will improve the charge separation which will increase the photocatalytic activity.

As shown in Fig. 6, the absorption properties of the samples are measured by UV–visible spectroscopy and found that all the samples show the characteristic spectrum with their fundamental absorption sharp edge. From the curves of $(\alpha hv)^2$ versus hv derived from the UV–visible spectra, it is found that the pure ZnO almost exhibits the same band gap energy of 3.29 eV whether as prepared or being calcined at 200 °C, while the samples of ZnO–G prepared at 200 °C exhibit a gap energy of about 3.26 eV which is slightly smaller than 3.31 eV for ZnO–GO as prepared, which may also be deduced that the presence of graphene has some influence on the electronic energy level of ZnO nano-particles.

The PL emission (excited at 325 nm) spectra recorded at room temperature are also shown in Fig. 6. Pure ZnO as prepared shows three strong and wide PL peaks at about 410, 468 and 525 nm

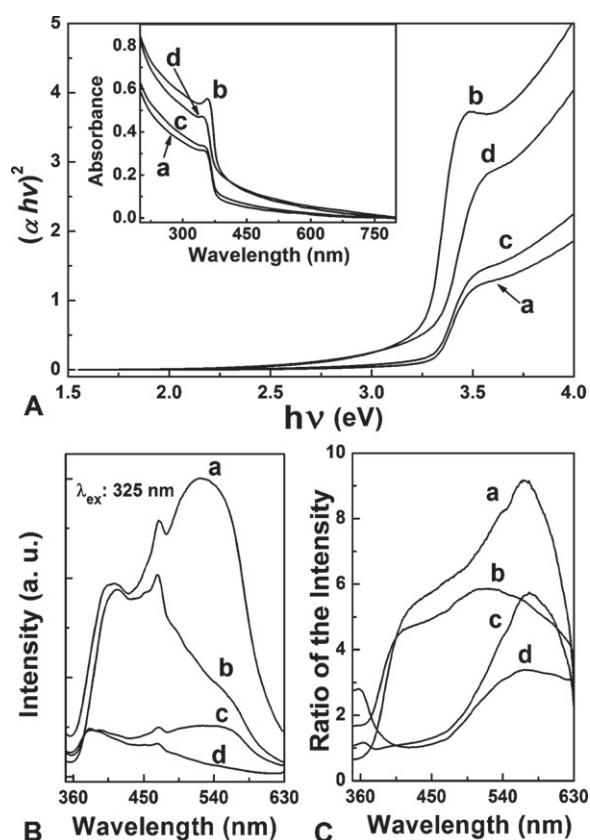


Fig. 6. (A) The plots of $(\alpha hv)^2$ versus hv derived from the UV–visible spectra (the inset) measured by using the dispersion of photo-catalyst: (a) ZnO–GO (2.5%) as prepared, (b) ZnO–G prepared at 200 °C, (c) pure ZnO as prepared and (d) thermally treated at 200 °C (B) the room temperature PL emission of the catalysts: (a) pure ZnO as prepared, (b) ZnO prepared at 200 °C, (c) the ZnO–GO as prepared and (d) ZnO–G prepared at 200 °C; (C) the ratio of PL intensity shown in (B): (a) I_b/I_d , (b) I_a/I_c , (c) I_c/I_d and (d) I_a/I_b .

although the band–band PL phenomenon cannot be found. The PL peak at 410 nm is attributed to band edge free excitons, while that at 468 nm is attributed to bound excitons [43], and that at 525 nm is resulted from the high-level surface defects which account for the increase of the green emission [44]. Currently, it is considered that ZnO nanostructures with a higher surface area to volume ratio might favor a high-level surface defects which account for the increase of the long wavelength emission [45–48]. The stronger emission at the long wavelength indicates that the ZnO as prepared exhibits many surface defects [49–51]. However, the ZnO–GO as prepared exhibits a blue-shifted peak at 390 nm, and a much weaker emission at 540 nm than pure ZnO as prepared. These may be resulted from the factors: (1) the presence of GO may be favorable to eliminate the defect of the ZnO particles which will make the near band edge emission blue shift, and (2) the GO can accept the photo-generated electrons which will cause a weaker emission. After thermally treated, the emissions' intensities at long wavelength become much weaker than pure ZnO and ZnO–GO as prepared, indicating that the thermal treatment is favorable for elimination of the surface defects. In order to illustrate the contribution of graphene in the hybrid materials, the relative intensity ratios among the PL spectra of the samples are shown in Fig. 3C, from which it can be seen clearly that the intensity of the emission band located at long wavelength in all samples changes dramatically either with graphene or thermal treatment. Furthermore, it can be deduced that the graphene exhibits higher ability to quench the emission at long wavelength than GO, and that the presence of graphene has larger ability to quench the emission than only thermal treatment by comparing the curve a with b, and curve c with d, respectively, indicating that the presence of graphene can accept the photo-induced electron assuredly and improve the charge separation.

3.2. Optimization based on the kinetics of photodegradation

It is well accepted that the photo-catalytic degradation of the organic pollutants follows the pseudo first-order kinetic [52], which exhibits a linear relationship between $\ln(C_0/C_t)$ and the reaction time. The kinetics equation of the first-order reaction can be described as:

$$\ln \frac{C_0}{C_t} = Kt \quad (1)$$

where C_0 is the initial concentration of MB, t the reaction time and C_t the concentration of MB at reaction time t . So based on the first-order equation the activities of the photo-catalysts are determined by measuring the absorbency of the MB in solution at a certain time intervals (Fig. S3). It shall be noted that the mixture of ethanol and water with a ratio of 3:1 in volume is used as medium to measure the absorbency of MB because of the strong congregation of MB in pure water (Fig. S4).

The control experiments such as the degradation of MB under radiation without photo-catalyst or under dark in the presence of photo-catalyst are carried out in order to get the sole influence of the light or photo-catalyst (Fig. S5). It can be clearly found that the degradation of the MB is slight without photo-catalyst, and the photo-catalyst has no more than 5% degradation for MB under the dark for 50 min.

The relationship between the apparent reaction constants (K_{app}) for the photo-degradation of MB in the presence of ZnO–G calcined at 200 °C and the content of graphene is shown in Fig. 7, it can be seen from which that the pure ZnO particles exhibit a K_{app} of about 0.035 min^{-1} , and that the K_{app} increases with the increment of graphene in samples of ZnO–G, and reaches to about 0.108 min^{-1} which is three times greater than that of pure ZnO when the content of graphene is 2.5% and obviously larger than that of commercial

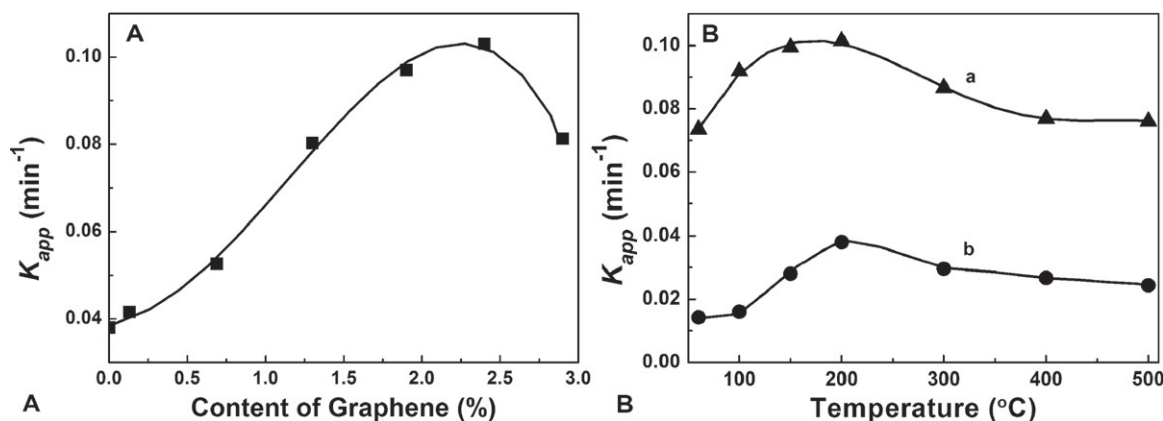


Fig. 7. The relationships of the apparent reaction constant K_{app} for MB degradation and the content of graphene in the hybrid materials of ZnO-G (A); the plots of K_{app} for MB degradation versus the temperature of thermal treatment for pure ZnO and ZnO-G containing 2.5% graphene (B). The content of photo-catalyst used in the system is 600 mg L⁻¹, and the concentration of MB is 20 mg L⁻¹ (50 mL).

P25 (0.066 min⁻¹) under the same condition (Fig. S6). In order to compare the influence of the supports, the ZnO-MWCNT composite has also been synthesized in similar procedure and the activity is determined under the same condition, it is found that the K_{app} (0.044 min⁻¹) is obviously smaller than that of ZnO-G (Fig. S7). However, the K_{app} for MB degradation decreases when the content of graphene in ZnO-G is larger than 2.5%, so the sample of ZnO-G containing 2.5% graphene is chosen in the following experiments. The decrement of the activity at higher content of graphene may be attributed to the increased absorbance and scattered photons through excess graphene in the system.

From Fig. 7B which shows the plots of K_{app} for MB degradation versus the temperature of thermal treatment, it is clear that the pure ZnO and ZnO-G exhibit the highest K_{app} when the samples are thermally treated at 200 °C. Furthermore, the K_{app} boosts up gradually with an increment of temperature under 200 °C while decreases gradually when the temperature is higher than 200 °C. During the thermal treatment, the water and some organic matters will be eliminated, the crystalline will be improved, the GO structure will be changed to form the graphene, and the ZnO particles will contact graphene sheets more intimately, so the K_{app} increases under 200 °C. However, the size of particles will become larger dramatically with the increment of the temperature, which will decrease the specific surface area. It has been proved that the rate of the charge movement will increase and the recombination probability of the hole-electron pairs will become lower in the

semiconductor due to the small size, which leads to the increase of the photo-catalytic efficiency.

3.3. Photocatalytic degradation

Fig. 8A shows that the photo-degradation rate of MB increases with the increment of the amount of ZnO-G prepared at 200 °C in the solution. It shall be noted that MB can only be degraded slightly (12.5%) under the radiation without the photo-catalyst, while noticeable degradation of MB has occurred when the concentration catalyst is only 50 mg L⁻¹ and increases with the increment of ZnO-G. The K_{app} for MB photo-degradation without photo-catalyst is about 0.0026 min⁻¹ and increases dramatically with the increment of the catalyst in the solution, furthermore, the K_{app} increases almost linearly in the catalyst content range of 100–600 mg L⁻¹ except that the K_{app} increases relatively quickly when the content of catalyst is <100 mg L⁻¹, and increases relatively slowly when the content of the catalyst is >600 mg L⁻¹. This result indicates that the low content of catalyst cannot absorb the light completely, so the K_{app} increases quickly in low concentration; however, the incident light may be reflected by the excess catalyst particles when the content is much higher.

The influence of OH⁻ ion on the photo-degradation of MB has also been investigated in the solutions with different pH values (Fig. 9). It can be seen that the degradation rate of MB increases with the increment of pH value when the content of ZnO-G prepared is

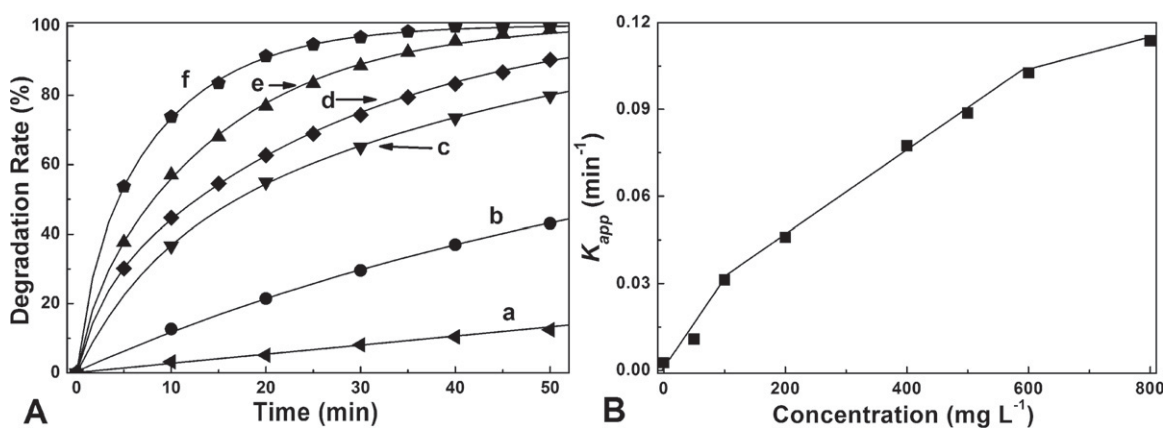


Fig. 8. (A) The curves of the degradation of MB in the presence of ZnO-G prepared at 200 °C at different contents in the solution of MB: (a) 0, (b) 50, (c) 100, (d) 200, (e) 400 and (f) 800 mg L⁻¹; (B) the plot of K_{app} versus the content of ZnO-G in the solution of MB. The concentration of MB is 20 mg L⁻¹ (50 mL).

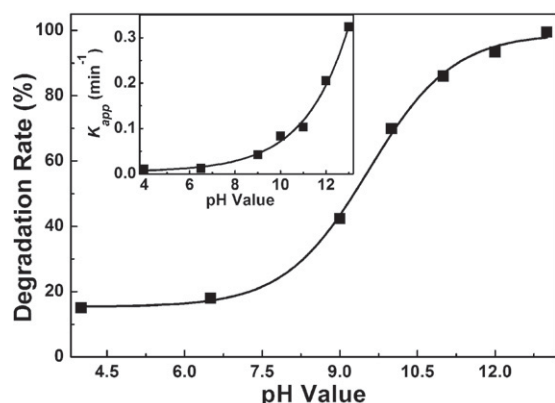


Fig. 9. The plot of the degradation rate of MB in the presence of ZnO–G versus pH, the concentration of MB is 20 mg L^{-1} (50 mL), and the content of the ZnO–G prepared at 200°C is 50 mg L^{-1} .

kept at 50 mg L^{-1} and the reaction time is 14.0 min at room temperature, respectively. Initially, the K_{app} increases slowly with the increment of pH value in the low pH region while the K_{app} increases dramatically in the larger pH region. This may be contributed to the fact that the change of pH has affected the adsorption behavior of MB which bears positive ion on the surface of photo-catalyst where hydroxy base has carried more negative charges (Fig. S8). On the other hand, OH^- may also act as the capture reagent of h^+ :



where $\cdot\text{OH}$, as oxidized material of photochemical catalysis, will be decreased by other materials (such as response intermediate, resultant, inorganic ions etc.) which have an intense adsorption on the surface of catalyst. So the increase of pH makes reduction of the recombination probability of electron and hole, which will make the photocatalytic activity enhanced [53].

In order to obtain the activity under irradiation of visible light (400–600 nm), the degradation of the dye is examined under the same procedure except that the UV light is cut off by a filter. It is found that the degradation rate of MB is very small for both the pure ZnO (12%) and ZnO–G (11%) in 50 min, which is slightly larger than that for visible light solely (7%) and indicates that the degradation is mainly resulted from the UV light (Fig. S9).

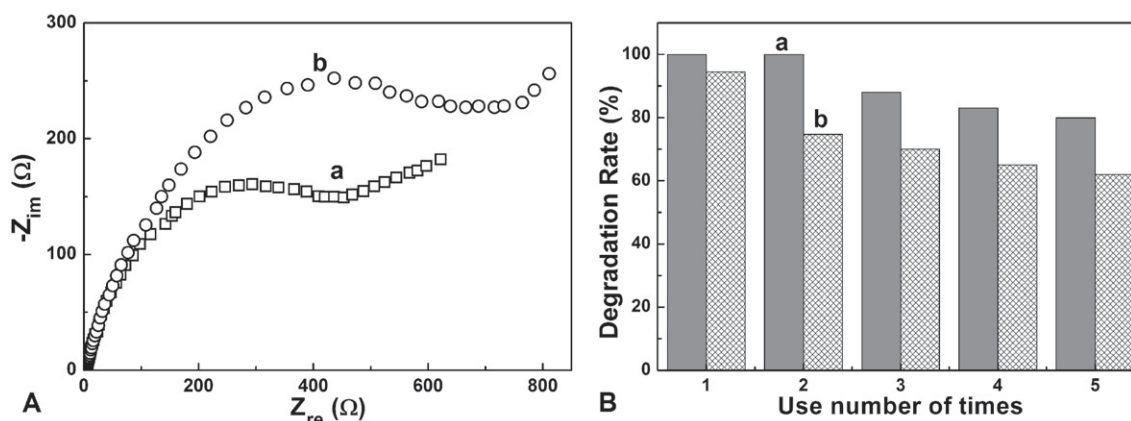


Fig. 10. (A) EIS properties of the electrodes decorated with ZnO–G (a) and pure ZnO prepared at 200°C (b). The EIS measurements were performed in the presence of a $2.5 \text{ mM K}_3[\text{Fe}(\text{CN})_6]/\text{K}_4[\text{Fe}(\text{CN})_6]$ (1:1) mixture as a redox probe in 0.1 M KCl aqueous solution. (B) The influence of catalyst use number of times on activeness of photochemical catalyst (a) ZnO–G and (b) pure ZnO prepared at 200°C .

3.4. EIS measurement and recycled properties

It is well known that graphene is the excellent electron acceptor and transporter due to its two-dimensional conjugation structure. So in ZnO–G system graphene will serve as an acceptor of the generated electrons of ZnO and can effectively suppress the charge recombination, leaving more charge carriers to form reactive species and promote the degradation of dyes. As shown in Fig. 10A, the typical electrochemical impedance spectra are presented as Nyquist plots, and it is observed that the semicircle in the plot becomes smaller with the introduction of graphene in small amount, which indicates a decrement of resistance in the solid state interface layer and the charge transfer on the surface. Overall, both the electron accepting and transporting properties of graphene in the hybrid could contribute to the suppression of charge recombination, and thereby a higher rate in the photocatalysis will be achieved.

The recycled properties of the catalyst ZnO–G and ZnO prepared at 200°C are also measured in 50 mL MB solution (20 mg L^{-1}) containing 30 mg catalyst. Keeping the condition of photo-catalytic degradation invariable, the identical catalyst is to be used 1, 2, 3, 4, 5 times separately under the radiation of 70 min each time. From the results shown in Fig. 10B, changes of degradation rate are observed from the relationship between the number of times of reuse and the photodegradation rate. The experiments indicate that the ZnO–G prepared at 200°C can still retain 80% activity for degradation of MB after repeated uses of 5 times, and exhibits larger degradation rate than pure ZnO in every recycled time, indicating that it can be reused.

The microstructure changes have also been investigated by comparing the SEM images of the catalyst before and after 5 times' repeated uses (Fig. 11). It is found that pure ZnO particles exhibit a slight aggregation in initial condition, but obvious aggregation has occurred after five times' repeated uses. For the catalyst of ZnO–G, it is surprising to find that some ZnO particles have peeled off the graphene sheets after 5 times' repeated uses although the surface of graphene sheets is coated with ZnO particles uniformly in relatively high density during initial stage.

From the above-mentioned experiment results, it can be deduced that the high enhance of the photodegradation of ZnO–G may come from the following: such structural changes of ZnO as the big lattice constants, small particles size and the small band gap energy may be favorable for the adsorption of MB on the catalyst surface and the utilization of the light radiation; on the other hand, the graphene has been reported to be a competitive candidate for the acceptor material due to its two-dimensional conjugation

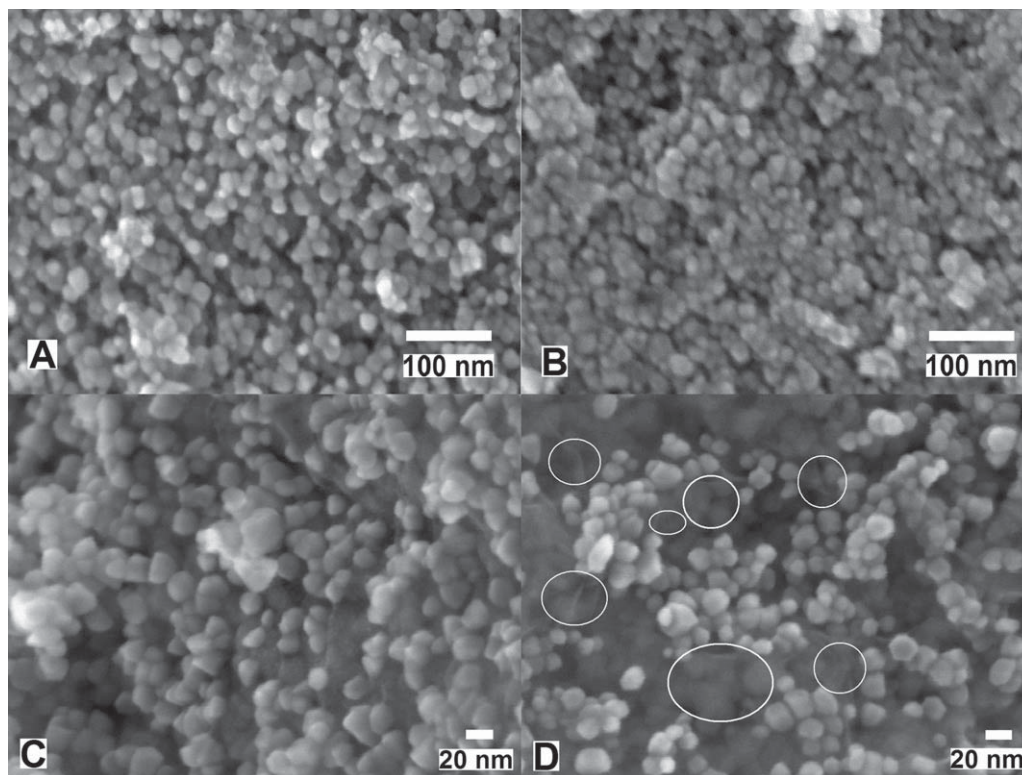


Fig. 11. The SEM images of the ZnO prepared at 200 °C (A) and (B), ZnO–G prepared at 200 °C (C) and (D), before photo-catalytic degradation of MB (A) and (C) and after the photo-degradation of MB for 5 times (B) and (D).

structure [54], and in the ZnO–G system, the excited electrons of ZnO could transfer from the conduction band to graphene, therefore an effective charge separation can be accomplished [55], which make more charge carriers form reactive species and promote the degradation of MB.

However, the ZnO particles will peel off the graphene sheets, the structure of graphene will also be destructed slowly during the durability test, which will cause the process of charge separation suffocated; moreover, the impurity or the inorganic ions will occupy the photo-catalyst active centers and change the structure of the catalyst. The above-mentioned factors may be part of the reasons for the deactivating of catalyst.

4. Conclusions

ZnO supported on graphene sheets can improve the photo-catalytic performance. The structure of the ZnO may be changed obviously in the presence of graphene and the photo-catalytic efficiency of the system is significantly influenced by the calcining temperature and the graphene content. The nano-ZnO supported on graphene sheets not only solve the dispersing problem but have a positive synergistic effect on the ZnO photocatalysis. It is proved that the ZnO–G hybrid can be used as photocatalysts for environmental remedial applications. The ZnO–G hybrid is easy to be gathered and recycled.

Acknowledgments

The authors thank the National Natural Science Foundation of China (21073115, 20604014), Natural Science Foundation (2007021008) of Shanxi province, the Program for New Century Excellent Talents in University (NCET-10-0926) of China and the Program for the Top Young and Middle-aged Innovative Talents of Higher Learning Institutions of Shanxi province (TYMIT and TYAL).

Appendix A. Supplementary data

Supplementary data associated with this article can be found, in the online version, at doi:10.1016/j.matchemphys.2011.11.085.

References

- [1] A. Mills, S.L. Hunte, *J. Photochem. Photobiol. A: Chem.* 108 (1997) 1.
- [2] K.I. Hadjiivanov, D.G. Klissurski, *Chem. Soc. Rev.* 25 (1996) 61.
- [3] A. Heller, *Acc. Chem. Res.* 28 (1995) 503.
- [4] K. Gouvea, F. Wypych, S.G. Moraes, N. Duran, N. Nagata, P. Peralta-Zamora, *Chemosphere* 40 (2000) 433.
- [5] B. Dindar, S. Icli, *J. Photochem. Photobiol. A: Chem.* 140 (2001) 263.
- [6] S. Sakthivel, S.U. Geissen, D.W. Bahnemann, V. Murugesan, A. Vogelpohl, *J. Photochem. Photobiol. A: Chem.* 148 (2002) 283.
- [7] Y.X. Wang, X.Y. Li, N. Wang, X. Quan, Y.Y. Chen, *Sep. Purif. Technol.* 62 (2008) 727.
- [8] D. Barreca, A. Gasparotto, C. Maccato, E. Tondello, U.L. Stangar, S.R. Patil, *Surf. Coat. Technol.* 203 (2009) 2041.
- [9] M.R. Hoffmann, S.T. Martin, W. Choi, D.W. Bahnemann, *Chem. Rev.* 95 (1995) 69.
- [10] W.G. Xu, S.F. Liu, S.X. Lu, S.Y. Kang, Y. Zhou, H.F. Zhang, *J. Colloid Interface Sci.* 351 (2010) 210.
- [11] T. Hirakawa, P.V. Kamat, *J. Am. Chem. Soc.* 127 (2005) 3928.
- [12] S.H. Elder, F.M. Cot, Y. Su, S.M. Heald, A.M. Tyryshkin, M.K. Bowman, Y. Gao, M.L. Balmer, A.C. Kolwaite, K.A. Magrini, D.M. Blake, *J. Am. Chem. Soc.* 122 (2000) 5138.
- [13] H.B. Fu, T.G. Xu, S.B. Zhu, Y.F. Zhu, *Environ. Sci. Technol.* 42 (2008) 8064.
- [14] H. Zhang, R.L. Zong, Y.F. Zhu, *J. Phys. Chem. C* 113 (2009) 4605.
- [15] K. Woan, G. Pyrgiotakis, W. Sigmund, *Adv. Mater.* 21 (2009) 2233.
- [16] L.W. Zhang, H.Y. Cheng, R.L. Zong, Y.F. Zhu, *J. Phys. Chem. C* 113 (2009) 2368.
- [17] X.G. Chen, Y.Q. He, Q. Zhang, L.J. Li, D.H. Hu, T. Yin, *J. Mater. Sci.* 45 (2010) 953.
- [18] C. Berger, Z. Song, X. Li, X. Wu, N. Brown, C. Naud, D. Mayou, T. Li, J. Hass, A.N. Marchenkov, E.H. Conrad, P.N. First, W.A. de Heer, *Science* 312 (2006) 1191.
- [19] S. Stankovich, D.A. Dikin, G.H.B. Dommett, K.M. Kohlhaas, E.J. Zimney, E.A. Stach, R.D. Piner, S.T. Nguyen, R.S. Ruoff, *Nature* 442 (2006) 282.
- [20] S.J. Park, R.S. Ruoff, *Nat. Nanotechnol.* 4 (2009) 217.
- [21] H. Zhang, X. Lv, Y. Li, Y. Wang, J.H. Li, *ACS Nano* 4 (2010) 380.
- [22] J.L. Wu, X.P. Shen, L. Jiang, K. Wang, K.M. Chen, *Appl. Surf. Sci.* 256 (2010) 2826.
- [23] X.Y. Zhang, H.P. Li, X.L. Cui, Y.H. Lin, *J. Mater. Chem.* 20 (2010) 2801.

- [24] G. Williams, P.V. Kamat, *Langmuir* 25 (2009) 13869.
- [25] T.N. Lambert, C.A. Chavez, B. Hernandez-Sanchez, P. Lu, N.S. Bell, A. Ambrosini, T. Friedman, T.J. Boyle, D.R. Wheeler, D.L. Huber, *J. Phys. Chem. C* 113 (2009) 19812.
- [26] O. Akhavan, E. Ghaderi, *J. Phys. Chem. C* 113 (2009) 20214.
- [27] N.L. Yang, J. Zhai, D. Wang, Y.S. Chen, L. Jiang, *ACS Nano* 4 (2010) 887.
- [28] S.R. Kim, M.K. Parvez, M. Chhowalla, *Chem. Phys. Lett.* 483 (2009) 124.
- [29] Y.B. Tang, C.S. Lee, J. Xu, Z.T. Liu, Z.H. Chen, Z.B. He, Y.L. Cao, G.D. Yuan, H.S. Song, L.M. Chen, L.B. Luo, H.M. Cheng, W.J. Zhang, I. Bello, S.T. Lee, *ACS Nano* 4 (2010) 3482.
- [30] T.G. Xu, L.W. Zhang, H.Y. Cheng, Y.F. Zhu, *Appl. Catal. B: Environ.* 101 (2011) 382.
- [31] Y.X. Xu, H. Bai, G.W. Lu, C. Li, G.Q. Shi, *J. Am. Chem. Soc.* 130 (2008) 5856.
- [32] Y.X. Xu, Q. Wu, Y.Q. Sun, H. Bai, G.Q. Shi, *ACS Nano* 4 (2010) 7358.
- [33] M.E. Wong, J.E. Bonevich, P.C. Searson, *J. Phys. Chem. B* 102 (1998) 7770.
- [34] F.K. Shan, B.I. Kim, G.X. Liu, Z.F. Liu, J.Y. Sohn, W.J. Lee, B.C. Shin, Y.S. Yu, *J. Appl. Phys.* 95 (2004) 4772.
- [35] D.X. Yang, A. Velamakanni, G. Bozoklu, S. Park, M. Stoller, R.D. Piner, S. Stankovich, I. Jung, D.A. Field, C.A. Ventrice Jr, R.S. Ruoff, *Carbon* 47 (2009) 145.
- [36] F. Wang, K. Zhang, *J. Mol. Catal. A: Chem.* 345 (2011) 101.
- [37] J.C. Liu, H.W. Bai, Y.J. Wang, Z.Y. Liu, X.W. Zhang, D.D. Sun, *Adv. Funct. Mater.* 20 (2010) 4175.
- [38] U. Zielke, K.J. Huttinger, W.P. Hoffman, *Carbon* 34 (1996) 983.
- [39] X.G. Han, H.Z. He, Q. Kuang, X. Zhou, X.H. Zhang, T. Xu, Z.X. Xie, L.S. Zheng, *J. Phys. Chem. C* 113 (2009) 584.
- [40] S. Stankovich, D.A. Dikin, R.D. Piner, K.A. Kohlhaas, A. Kleinhammes, Y.Y. Jia, Y. Wu, S.T. Nguyen, R.S. Ruoff, *Carbon* 45 (2007) 1558.
- [41] E.P. Gao, W.Z. Wang, M. Shang, J.H. Xu, *Phys. Chem. Chem. Phys.* 13 (2011) 2887.
- [42] E.J. Yoo, T. Okata, T. Akita, M. Kohyama, J. Nakamura, I. Honma, *Nano Lett.* 9 (2009) 2255.
- [43] L.Q. Jing, Y.C. Qu, B.Q. Wang, S.D. Li, B.J. Jiang, L.B. Yang, *Sol. Energy Mater. Sol. Cells* 90 (2006) 1773.
- [44] Y.W. Chen, Q. Qiao, Y.C. Liu, G.L. Yang, *J. Phys. Chem. C* 113 (2009) 7497.
- [45] D.A. Van, E.A. Meulenkaamp, *J. Lumin.* 87–89 (2000) 454.
- [46] K. Vanheusden, W.L. Warren, C.H. Seager, D.R. Tallant, J.A. Voigt, B.E. Gnade, *J. Appl. Phys.* 79 (1996) 7983.
- [47] X.T. Zhang, Y.C. Liu, J.Y. Zhang, Y.M. Lu, D.Z. Shen, X.W. Fan, X.G. Kong, *J. Cryst. Growth* 254 (2003) 80.
- [48] B.L. He, B. Dong, H.L. Li, *Electrochem. Commun.* 9 (2007) 425.
- [49] P. Yang, H.Q. Yan, S. Mao, R. Russo, J. Johnson, R. Saykally, N. Morris, J. Pham, R.R. He, H. Choi, *Adv. Funct. Mater.* 12 (2002) 323.
- [50] M.H. Huang, Y.Y. Wu, P.D. Yang, *Adv. Mater.* 13 (2001) 113.
- [51] Q. Tang, W.J. Zhou, J.M. Shen, W. Zhang, L.F. Kong, Y.T. Qian, *Chem. Commun.* 6 (2004) 712.
- [52] Y.J. Li, X.D. Li, J.W. Li, J. Yin, *Water Res.* 40 (2006) 1119.
- [53] K.S. Novoselov, A.K. Geim, S.V. Morozov, D. Jiang, Y. Zhang, S.V. Dubonos, I.V. Grigorieva, A.A. Firsov, *Science* 306 (2004) 666.
- [54] Q. Liu, Z.F. Liu, X.Y. Zhang, L.Y. Yang, N. Zhang, G.L. Pan, S.G. Yin, Y.S. Chen, J. Wei, *Adv. Funct. Mater.* 19 (2009) 894.
- [55] X. Wang, L.J. Zhi, K. Mullen, *Nano Lett.* 8 (2008) 323.